ACS APPLIED MATERIALS & INTERFACES

Research Article

www.acsami.org

# Reduced Graphene Oxide Supported Palladium Nanoparticles via Photoassisted Citrate Reduction for Enhanced Electrocatalytic Activities

Yu-Xi Huang, Jia-Fang Xie, Xing Zhang, Lu Xiong, and Han-Qing Yu*

CAS Key Laboratory of Urban Pollutant Conversion, Department of Chemistry, University of Science & Technology of China, Hefei 230026, China

Supporting Information

**ABSTRACT:** Reduced graphene oxide (rGO) supported palladium nanoparticles (Pd NPs) with a size of ~3 nm were synthesized using one-pot photoassisted citrate reduction. This synthetic approach allows for the formation and assembly of Pd NPs onto the rGO surface with a desired size and can be readily used for other metal NP preparation. The prepared rGO-Pd exhibited 5.2 times higher mass activity for ethanol oxidation reaction than the commercial platinum/carbon (Pt/C). In the oxygen reduction reaction tests, rGO-Pd exhibited comparable activity compared with Pt/C and maintained its high performance after 4000 cycles of potential sweep. These results demonstrate that our synthetic approach is effective for preparing graphene-supported metal NPs with excellent activity and stability in ethanol oxidation and oxygen reduction reactions.

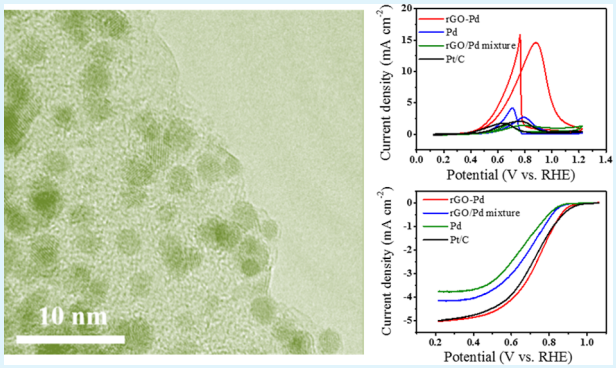


**KEYWORDS:** *reduced graphene oxide, palladium nanoparticle, photoassisted citrate reduction, oxygen reduction reaction, ethanol oxidation reaction*

## INTRODUCTION

Graphene- and graphene oxide (GO)-based nanocomposites have emerged as new star materials after the discovery of graphene.[1−5] Because of their extraordinary physical and chemical properties, graphene/GO-based nanocomposites have been explored extensively for various applications, such as electronic devices, batteries, supercapacitors, fuel cells, and electrocatalysts.[6−12] Graphene and GO are widely used as excellent carbon supports for catalysts to achieve the desired activity and stability. For example, it has been reported that graphene/GO-supported metal or metal oxide nanoparticles (NPs) could improve the performance of catalysts in oxygen reduction reaction (ORR), hydrogen evolution reaction, and oxygen evolution reaction.[9,13−17] Theoretical calculations have shown that the interaction between metal and graphene would change the Fermi level of both the metal and graphene, which plays an important role in enhancing the catalytic activity.[18,19] Thus, it is of great interest to prepare graphene/GO-based metal NPs with excellent catalytic activity.

Currently, two approaches have been widely used to synthesize graphene/GO-supported metal NPs, i.e., an in situ growth method and an ex situ assembly method.[3] The ex situ assembly approach usually needs surface modification of the NPs and/or graphene/GO, so that they can bind together through noncovalent interactions or chemical bonding.[7,13,14,19−21] However, the ex situ method often suffers from the complicated modification process and nonuniform coverage of NPs on graphene/GO surfaces. In contrast, the in situ growth approach offers the opportunity of one-pot synthesis of graphene/GO-based composites in different ways, such as chemical reduction, hydrothermal reduction, and electrochemical deposition. However, in order to obtain well-dispersed NPs on the graphene/GO surface with the desired size and morphology, surfactants are needed and sophisticated reaction control should be employed, which limits the further application of this approach.[8,9,15,16,20−28] Hence, it is highly desired to find an easier and cleaner way to synthesize graphene/GO-supported metal NPs.

Recently, photochemical and photothermal reduction methods have been developed to prepare metal NPs on different supports.[22,25−27,29−32] For example, noble metal NPs such as gold (Au), platinum (Pt), palladium (Pd), and silver (Ag) can be synthesized on a graphene or ZnO support under laser or UV illumination. The site-specific growth of Au NPs on the ZnO nanopyramids and the formation mechanism have been reported.[32] In these studies, laser illumination and/or semiconductor support is usually used, and the size distribution of the obtained NPs usually needs further optimization. As a

Received: May 8, 2014
Accepted: August 25, 2014
Published: August 25, 2014

  

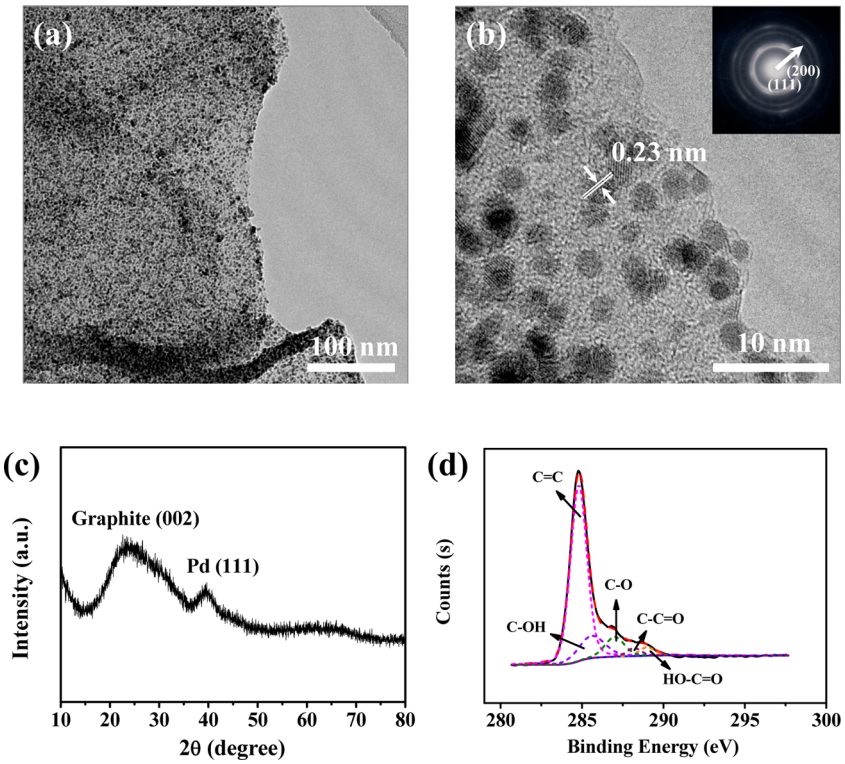


**Figure 1.** TEM image (a), HRTEM image (b), XRD pattern (c), and C 1s XPS spectrum (d) of the as-prepared rGO-Pd.

result, the catalytic potentials of the prepared materials may not be fully realized. Nevertheless, such a strategy approach provides an opportunity for the in situ growth of metal NPs on graphene under mild conditions. To better control the dispersity and size distribution of the metal NPs in the photoreduction system, one would expect that by introducing a moderate reducing agent, the metal ions could nucleate and grow mildly on the GO support to avoid undesirable agglomeration. In this way, GO would also be reduced to reduced graphene oxide (rGO) in the presence of reductant and illuminant, consequently forming rGO-supported metal NPs.

In this study, we proposed a facile and universal synthetic approach to fabricate rGO-supported Pd NPs by using photoassisted citrate reduction. The Pd precursor and GO could be reduced simultaneously, forming well-dispersed 3 nm Pd NPs assembled on rGO (rGO-Pd). This synthetic method offers a facile way to prepare rGO/metal NP nanocomposites with well size distribution. The obtained rGO-Pd exhibited excellent electrochemical activity and stability in electrochemical ethanol oxidation reaction (EOR) and ORR.

## MATERIALS AND METHODS

**Preparation of GO.** Chemicals used in our work were purchased from Sinopharm Chemical Reagent Co., China, and used without further purification, unless otherwise specified. GO was prepared using a modified Hummers method.[33,34] Briefly, 0.5 g of graphite powders (<30 $\mu$m) and 0.5 g of $NaNO_3$ were stirred with 23 mL of concentrated $H_2SO_4$ in an ice bath. Then, 3 g of $KMnO_4$ was added slowly within 10 min. In the subsequent 1 h, the mixture was maintained in 35 °C with vigorous stirring. After that, 40 mL of deionized water was dosed into the reaction mixture and further heated to 90 °C for 30 min. Thereafter, the mixture was removed from the water bath, and 100 mL of water was added. The unreacted $KMnO_4$ and residual manganese species were removed by the addition of 3% $H_2O_2$. The suspension was stirred at room temperature for 4 h and purified by repeated centrifugation until a negative reaction on the sulfate ion [with $Ba(NO_3)_2$] was achieved. The final precipitate was dispersed in 50 mL of water and ultrasonicated for 10 min. The insoluble solids were crushed by centrifugation at 3000*g* for 5 min, and a brown homogeneous supernatant was collected. The concentration of the GO solution was 4.65 mg $mL^{-1}$, determined by drying the solution in an oven at 60 °C.

**Preparation of rGO-Pd, a rGO/Pd Mixture, and Pd NPs.** To prepare rGO-Pd, 0.1 mL of the as-prepared GO solution, 5 mg of $Na_2PdCl_4$ (Aladdin Reagent Inc., China), and 0.5 g of sodium citrate were added to 49.8 mL of deionized water (18.2 MΩ cm). The solution was then transferred into a quartz bottle, purged with $N_2$, and sealed. A 500 W high-pressure mercury lamp was used as the light source. The solution was irradiated for 12 h, and the products were collected by filtration and washed with water, ethanol, and isopropyl alcohol. For the preparation of a rGO/Pd mixture and Pd NPs, the same method was used except that rGO and Pd NPs were synthesized separately and then mixed and ultrasonicated for 10 min. Thus, a rGO/Pd mixture was obtained. The final products were ultrasonically dispersed in isopropyl alcohol containing 0.05% Nafion (D520, Du Pont Inc., USA) for electrochemical tests. Both rGO-Au and rGO-Pt were prepared using a procedure similar to that for the preparation of rGO-Pd, except that 10 mg of gold(III) chloride trihydrate and 4 mg of sodium tetrachloroplatinate(II) hydrate were respectively used as the precursors.

**Characterization.** X-ray diffraction (XRD) tests were carried out on Rigaku TTR-III (Rigaku Corp., Japan) with Cu K$\alpha$ radiation. Transmission electron microscopy (TEM) images of the materials were obtained with a JEOL-2010 high-resolution transmission electron microscope (JEOL Ltd., Japan). The thicknesses of the obtained GO and rGO-Pd were measured using an atomic force microscope (DI MultiMode, Bruker Inc., USA). X-ray photoelectron spectroscopy (XPS) analysis was performed using an ESCALAB 250 instrument (Thermo-VG Scientific Inc., USA) with a monochromatic Al K$\alpha$ X-ray source. Raman spectra were obtained using a LABRAM-HR Raman spectrometer (JY Co., France) with an excitation wavelength of 514.5 nm generated by an $Ar^+$ laser. Fourier transform infrared (FTIR)

spectroscopy studies were conducted with a VERTEX 70 FTIR spectrometer (Bruker Inc., USA). UV−vis absorption spectra were acquired using a UV-2450 UV−vis spectrophotometer (Shimadzu Co., Japan) in a range of 200−800 nm. Inductively coupled plasma atomic emission spectroscopy (ICP-AES) measurements were conducted on an Optima 7300 DV spectrometer (PerkinElmer Co., USA).

**Electrochemical Tests.** The glassy carbon (GC) working electrode (5 mm diameter; Pine Instrument, USA) was first polished with 0.3 and 0.05 $\mu$m alumina powder and then ultrasonically cleaned in water. Electrochemical polishing was conducted in a 0.5 M $H_2SO_4$ solution using cyclic voltammetry (CV) scanned from −0.8 to 1.2 V (vs RHE) to further clean the surface of the GC electrode. Then, 20 $\mu$L of catalyst ink was dropped onto the electrode and dried at ambient temperature. The mass ratio of Pd NPs to rGO was determined to be around 2:1 by ICP-AES. The Pd loading amount of the catalysts was controlled at 25 $\mu$g cm$^{-2}$. All electrochemical measurements were conducted in a standard three-electrode system. The electrochemically active surface areas (ECSAs) of the catalysts were calculated according to the method proposed in the literature.[35] CV scans were conducted in 0.1 M KOH at a scan rate of 50 mV s$^{-1}$ with different upper potential limits from 0.96 to 1.46 V.

Electrocatalytic oxidation of ethanol was conducted in a solution containing 1 M ethanol and 1 M KOH at a scan rate of 50 mV s$^{-1}$ under a $N_2$ atmosphere. Chronoamperometric curves were recorded at 0.63 V for 2000 s. ORR tests were conducted in an oxygen-saturated solution containing 0.1 M KOH at a scan rate of 5 mV s$^{-1}$ and a rotation rate of 1600 rpm. Stability tests were carried out with potential cycles from 0.36 to 0.86 V at a scan rate of 50 mV s$^{-1}$ for 4000 cycles.

## RESULTS AND DISCUSSION

The TEM images in Figure 1 reveal that Pd NPs with a size of ∼3 nm were well-dispersed on the surface of rGO without aggregation. The high-resolution TEM (HRTEM) image (Figure 1b) shows the crystal lattice fringes throughout the several Pd NPs formed on rGO. The continuous lattice fringes exhibit an interplanar lattice spacing of ∼0.23 nm and match well with the (111) atomic planes of the face-centered-cubic (fcc) Pd. The inset in Figure 1b is the corresponding selected area electron diffraction (SAED) pattern, which shows the polycrystalline characteristics of Pd. The XRD pattern also reveals the typical pattern of fcc Pd(111) after the reaction (Figure 1c). The thicknesses of the obtained GO and rGO-Pd were measured using atomic force microscopy (AFM). Figure S1 in the Supporting Information (SI) shows that the thickness of GO was about 1.1 nm, while the size of Pd NPs on the rGO surface was around 2.7−3.0 nm, consistent with the TEM results.

rGO-Pd was further characterized by XPS, which was corrected with reference to the C 1s peak at 284.8 eV. As shown in Figure S2 in the SI, the binding energies of Pd 3d at 335.86 and 341.15 eV for rGO-Pd corresponded to the $Pd^0$ Pd $3d_{5/2}$ and Pd $3d_{3/2}$, respectively, confirming the presence of metallic Pd. In addition, a small amount of $Pd^{II}$ was identified in the XPS test, which corresponded to the surface oxidation of Pd. In addition, the C 1s spectrum of as-prepared GO showed a considerable degree of oxidation, which corresponded to the different functional groups (Figure S3a in the SI).[36] After photoassisted citrate reduction, the C 1s spectrum of rGO-Pd exhibited much smaller peak intensities for the oxygen functional groups, suggesting the reduction of GO (Figure 1d). In the Raman spectra shown in Figure S4 in the SI, both GO and rGO-Pd contained D and G bands, with a slightly increased D/G intensity for rGO-Pd compared to that for GO. This result suggests that the average size of $sp^2$ domains decreased upon the reduction of GO. This could be explained when new graphitic domains were formed during the reduction, which were smaller in size than the ones present in GO but more numerous in number.[37] Besides, the chemical interaction between the deposited Pd NPs and rGO may also break the $sp^2$ domain into smaller parts. The small peak located at 635 cm$^{-1}$ for rGO-Pd could be assigned to the surface PdO, which was confirmed by XPS.[38,39] Figure S5 in the SI shows the FTIR spectra of GO and rGO-Pd. The characteristic peaks for GO were the absorption bands corresponding to the C═O stretching at 1732 cm$^{-1}$, the aromatic C═C vibration at 1628 cm$^{-1}$, the O−H deformation vibration at 1400 cm$^{-1}$, the C−OH stretching at 1261 cm$^{-1}$, and the C−O stretching at 1075 cm$^{-1}$. The O−H stretching appeared at ∼3400 cm$^{-1}$ as a broad peak, and the peak at 1628 cm$^{-1}$ could also be assigned to the vibrations of the absorbed water.[40] After reduction, the relative intensities of these peaks were significantly reduced compared with the intensity of the aromatic C═C vibration peak located at 1628 cm$^{-1}$, suggesting the reduction of oxygenated functional groups such as −COOH, C−O−C, and C−OH.

To further investigate the role of illumination, control experiments were conducted. In the absence of UV illumination or under visible-light irradiation, neither GO nor Pd was reduced after 12 h, indicating that UV light was vital to the reduction process. This conclusion was further confirmed by UV−vis spectroscopy. As shown in Figure 2, $PdCl_4^{2-}$ has a

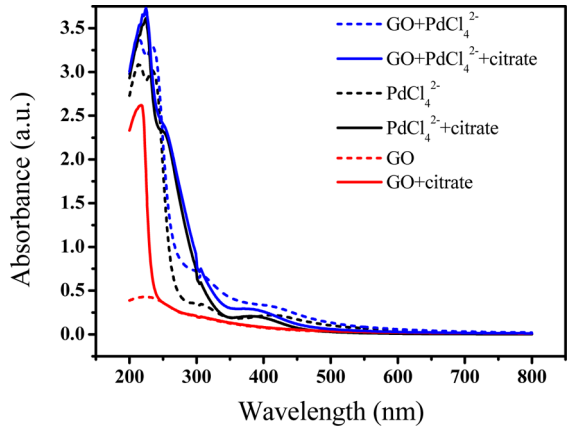


**Figure 2.** UV−vis absorption spectra of GO (red), $PdCl_4^{2-}$ (black), and GO + $PdCl_4^{2-}$ (blue) before (dashed line) and after (solid line) dosing with citrate.

strong absorption band in the UV region (from 200 to 270 nm) and a weak absorption peak at 415 nm. The absorption region of GO itself is weak and located from 200 to 400 nm. However, when $PdCl_4^{2-}$ and GO are mixed, a new broad absorption peak at around 305 nm appears, suggesting that the interaction between $PdCl_4^{2-}$ and GO occurs via partial replacement of the $Cl^-$ ion. After a dose of citrate, $PdCl_4^{2-}$ and $PdCl_4^{2-}$ + GO shows a new absorption peak at 250 nm, and GO also shows a strong absorption peak at 216 nm. These spectra indicate the coordination between citrate and $PdCl_4^{2-}$ or GO. When illumination is applied, the strong absorption in the UV region triggers the $Pd^{2+}$ and GO reductions because of the heat pulse generated by photothermal energy conversion.[26]

To further confirm this proposed mechanism, a control experiment had been conducted with the same recipe except that heating was used instead of illumination. The reaction was conducted at 90 °C for 26 h, as reported by Lim et al.[41] As

shown in Figure S6 in the SI, the small-sized aggregated Pd NPs were formed on the graphene surface. This result supports our proposed photothermal conversion mechanism. However, the heating approach needs much longer reaction time, and the productivity is much lower than that using illumination. These indicate that the reducing power offered by the photothermal conversion of GO was much stronger than that by the simple heating of the solution to 90 °C. On the other hand, in our system, a high-pressure mercury lamp was used as the light source without focus; thus, the illumination for a single reactor was not strong. The reaction time could be shortened if the illumination is increased.

For comparison, the Pd NPs synthesized with the same procedure became aggregated in the absence of GO (Figure S7a in the SI). The TEM image shows that the aggregated Pd NPs were about 40 nm in diameter, formed by much smaller Pd NPs. When such Pd NPs were mixed with rGO by ultrasonication, in the resulting rGO/Pd mixture, the aggregated Pd NPs were assembled on graphene (Figure S7b in the SI). This result implies the crucial role of GO as a growth substrate in this reaction.

To better reveal the Pd nucleate process during the formation of rGO-Pd, samples were taken for TEM imaging after 15 min, 1 h, 4 h, and 8 h of reaction. The TEM images indicate that the density of Pd NPs increased as the reaction proceeded, while the particle size did not change significantly, showing that a slow nucleate process occurred on the GO surface (Figure S8 in the SI). This could be explained by the Pd NP growth kinetics on the rGO surface. A recent theoretical study about the interaction between Pd atoms and the rGO surface suggests that Pd atoms would prefer to deposit and nucleate on the defect sites of graphene, a thermodynamically driven process as the defect sites could bind the Pd NP strongly. The Pd NP growth would finally reach equilibrium, and the resulting NPs would have a similar stability. In this case, the NP growth by the Ostwald ripening mechanism would be prohibited thermodynamically.[42] Thus, the Pd NP size did not change with the illumination time, while the NP density increased. In addition, without the help of citrate, illumination alone could not reduce $Pd^{II}$ to $Pd^{0}$; instead, PdO and partially reduced GO were obtained. The corresponding XPS and XRD results are shown in Figure S3b–d in the SI, which indicates that the presence of citrate was essential in this reaction.

On the basis of the above analysis, the growth process of Pd NPs on GO could be illustrated in Scheme 1. GO is highly negatively charged in aqueous solution because of its oxygenic functional groups and defects, which might favor the adsorption of Pd ions.[43] In the presence of citrate and illuminant, Pd ions became slowly nucleated and grew into small particles on the defect sites of GO, while the particle density increased slowly as well. GO itself was also reduced to rGO in this process. There was a strong anchoring effect between the Pd nuclei and the GO surface, resulting in separate nucleation of Pd NPs.[21] The slow growth rate in our case could also prevent overgrowth of the small Pd NPs; instead, well-dispersed Pd NPs with narrow size distribution could be readily obtained.

**Scheme 1. Scheme of the Formation Mechanism of rGO-Pd**

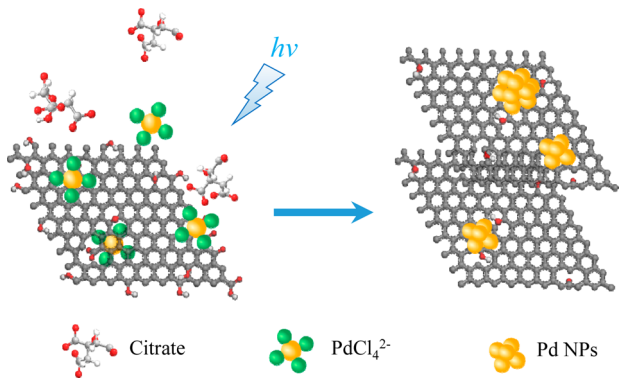


The catalysts were further tested in EOR and ORR. Figure 3 shows the typical CV curves of rGO-Pd, a rGO/Pd mixture, and Pd NPs in a $N_2$-saturated 0.1 M KOH solution. The onset reduction potentials of these three catalysts were similar, starting from about 0.85 V. However, the rGO/Pd mixture exhibited a broad reduction plateau in the potential region of 0.3–0.6 V, which corresponded to the electrochemical activity of rGO. In contrast, at a similar ratio of rGO and Pd, the CV pattern of rGO-Pd did not have the same electrochemical behavior as that of rGO in this region. Instead, rGO-Pd showed pure Pd behavior with larger double-layer capacitance compared to Pd NPs, indicating the presence of the rGO support.[5,44] This observation is interesting because rGO-Pd and the rGO/Pd mixture had the same chemical content. This result might be explained by the different preparation methods of these two samples. Considering that the rGO/Pd mixture was prepared by mixing and sonicating rGO and Pd NPs together, some of the Pd NPs were likely to be covered by rGO, preventing the reagent from accessing the Pd surface. In addition, because of the thin layer of palladium oxide on the Pd NP surface, when the Pd NPs were mixed with rGO, the interfacial interaction of these two components would not be as strong as that of rGO-Pd, resulting in poor interfacial interaction. These might result in an outstanding signal of rGO in the CV test.

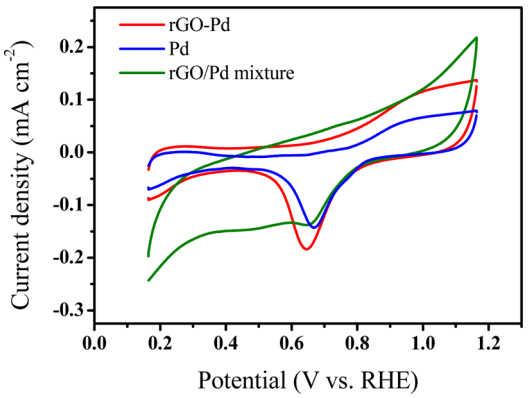


**Figure 3.** CV curves of rGO-Pd, a rGO/Pd mixture, and Pd NPs in 0.1 M KOH at a scan rate of 50 mV $s^{-1}$.

Then, the catalysts were tested for EOR in an electrolyte containing 1 M ethanol and 1 M KOH. The catalytic currents were normalized to the ECSAs and the loading amount of metals for comparison (Figure 4). A commercial Pt/C catalyst was also used as the standard. Figure 4a depicts the onset potential of ethanol oxidation on rGO-Pd, starting at around 0.3 V, which was lower than those for the Pd NPs and a rGO/Pd mixture. Moreover, rGO-Pd showed a remarkably larger current density than the other catalysts, including Pt/C (Figure 4a,b). The peak current densities obtained on rGO-Pd in positive and negative scans were 14.58 and 15.84 mA $cm^{-1}$,

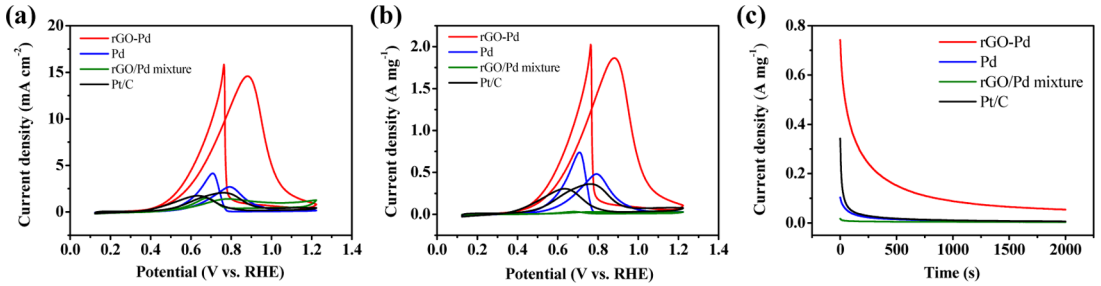


**Figure 4.** CV curves of rGO-Pd, a rGO/Pd mixture, Pd NPs, and commercial Pt/C in 1 M KOH in the presence of 1 M ethanol. The current densities were normalized to ECSAs (a) and mass (b), respectively. (c) Chronoamperometric curves for the catalysts at 0.63 V.

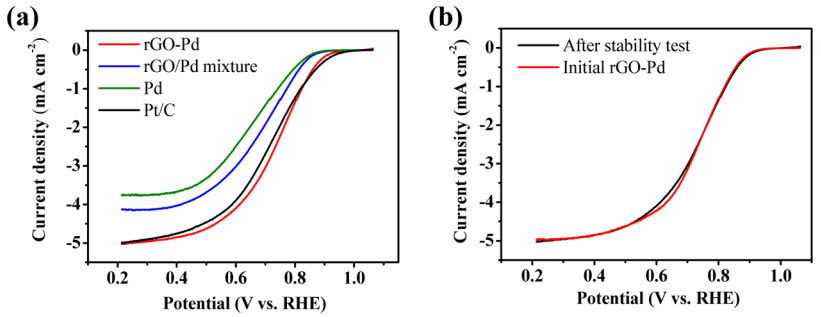


**Figure 5.** ORR polarization curves of rGO-Pd, a rGO/Pd mixture, Pd NPs, and commercial Pt/C in $O_2$-saturated 1 M KOH (a). Polarization curves of rGO-Pd before and after stability tests (b).

respectively, much higher than those on Pd NPs (2.70 and 4.14 mA cm$^{-1}$), rGO/Pd (1.40 and 1.49 mA cm$^{-1}$), and Pt/C (2.07 and 1.74 mA cm$^{-1}$). Furthermore, the mass current density of rGO-Pd reached about 2 A mg$^{-1}$ and was also better than those reported in the literature using similar Pd NPs, implying that the combination of rGO and Pd NPs could significantly enhance the catalytic activity. This result is consistent with recent reports on graphene-supported catalysts, in which the graphene could serve as an excellent NP support and enhance both the catalytic activity and stability.[21,44] Interestingly, as a control experiment, the rGO/Pd mixture seemed to have the lowest mass current density among all of the catalysts (Figure 4b). However, after the current density was normalized to the ECSA, the rGO/Pd mixture showed a similar level of current density compared with Pd NPs (Figure 4a). This result implies that most of the Pd NPs in the rGO/Pd mixture were not "electroactive", and utilization of Pd was not efficient in this way. As discussed above, the procedure for making the rGO/Pd mixture might result in rGO-coated Pd NPs and, consequently, a lower ECSA than that of pure Pd. Thus, the surface area activity of the rGO/Pd mixture was of a level similar to that of Pd and Pt/C, while its mass activity was lower. Recent reports reveal that graphene or GO is a good platform and plays an important role in the activity enhancement of the catalyst.[13,14] The improved performance of graphene-based composites relied on the rational assembly of the material and proper exposure of the active sites. Our result here confirms that it is of great importance to ensure good contact between the catalysts and graphene.

To evaluate the stability and long-term performance of our catalysts, chronoamperometric curves were recorded at 0.63 V for 2000 s. As shown in Figure 4c, rGO-Pd exhibited the highest current compared to the other catalysts, which is consistent with the CV results. All of the catalysts showed a rapid current decrease at the beginning of the chronoamperometric tests because of surface poisoning with the reaction intermediates.[45] Nevertheless, rGO-Pd showed a much higher mass current density than the others. After 2000 s, the current densities of rGO-Pd, a rGO/Pd mixture, Pd NPs, and Pt/C were 0.055, 0.004, 0.006, and 0.007 A mg$^{-1}$, respectively. This result further confirms the excellent performance of rGO-Pd.

In the ORR tests, the rotating-disk-electrode polarization curves of the catalysts were recorded in the $O_2$-saturated 0.1 M KOH solution. As shown in Figure 5a, rGO-Pd exhibited a comparable ORR activity toward the commercial Pt/C. The onset potential of ORR on rGO-Pd was slightly more negative than that on the Pt/C. However, the half-wave potential of rGO-Pd was 0.734 V, about 20 mV higher than that of the Pt/C, indicating that rGO-Pd has better kinetics than the Pt/C in ORR. On the other hand, the rGO/Pd mixture and Pd NPs showed much more negative onset potentials and half-wave potentials compared to rGO-Pd. The low ORR activities of the rGO/Pd mixture and Pd NPs should be due to the aggregation of Pd. However, the rGO/Pd mixture exhibited a better performance than pure Pd NPs, confirming that the rGO support could improve the electrochemical activity of the catalyst. The kinetic currents were calculated using the currents at 0.765 V in Figure 5a based on the Koutecký–Levich equation:

$$\frac{1}{i} = \frac{1}{i_k} + \frac{1}{i_d}$$

where $i_k$ is the kinetic current and $i_d$ is the diffusion-limiting current.

Table 1 summarizes the half-wave potentials and mass-kinetic currents of the prepared catalysts and further confirms that rGO-Pd had excellent ORR activity as the commercial Pt/C.

Stability tests were conducted with potential cycles from 0.36 to 0.86 V at a scan rate of 50 mV s$^{-1}$ for 4000 cycles. Figure 5b shows the ORR polarization curves for rGO-Pd before and after

Table 1. Comparison of the Half-Wave Potentials and Mass-Kinetic Currents at 0.765 V

| | $E_{1/2}$ (V vs RHE) | mass activity (mA $\mu g^{-1}$) |
|---|---|---|
| rGO-Pd | 0.734 | 0.088 |
| rGO/Pd mixture | 0.687 | 0.058 |
| Pd NPs | 0.657 | 0.068 |
| commercial Pt/C | 0.713 | 0.085 |

the stability test. Little change in the ORR activity was observed after 4000 potential cycles, while the rGO/Pd mixture and Pd NPs lost their activities significantly (Figure S9 in the SI).

The above EOR and ORR results have shown that rGO is an excellent carbon support for improving the activity and stability of Pd. Such an enhancement could be attributed to the tensile strain effect in the Pd layer when Pd contacts graphene. This effect results in electron exchange transfer between Pd and graphene interfaces and increases the interaction states and transmission channels between Pd and graphene while keeping sufficient $\pi$ electrons on graphene for conduction.[18] In the ORR process, the high overpotentials observed on most catalysts arise mainly from the strong adsorption of oxygen species. It has been reported that the electronic structure of Pd NP could be tuned by interaction with the defects on graphene, leading to weaker oxygen species adsorption strength and better ORR performance.[42,46,47] Because of the strong interaction between rGO and Pd, rGO-Pd exhibited excellent electrochemical activities for both EOR and ORR. On the other hand, lower activities were observed for the rGO/Pd mixture and Pd NPs, indicating that the tensile strain effect weakened as the Pd grew bigger on the graphene. In this case, the overgrowth Pd NPs tended to act as a "normal" Pd material rather than nanoscale contacts between small-sized Pd NPs and graphene.

Finally, we have extended this method to fabricate other rGO/metal nanocomposites. Figure S10 in the SI shows the TEM images of rGO-Au and rGO-Pt synthesized via an identical reduction process, confirming the universality of this synthetic strategy.

## CONCLUSIONS

In summary, by using one-pot photochemical citrate reduction of $PdCl_4^{2-}$ and GO, well-dispersed and assembled Pd NPs on a rGO support were synthesized. Owing to the surfactant-free synthesis process, the resulting materials do not need further surface washing or annealing. EOR and ORR tests revealed that the prepared rGO-Pd NPs had excellent catalytic activity and stability. Control experiments revealed that NPs should be assembled on the rGO surface properly to achieve improved electrochemical activity. This synthetic approach is effective for preparing rGO-supported Pd NPs in mild conditions without sophisticated reaction control and may also be readily applied to synthesize other rGO–metal NP composites like rGO-Pt and rGO-Au.

## ASSOCIATED CONTENT

### Supporting Information

AFM results, XPS, Raman, and FTIR spectra, TEM imgaes, and ORR curves. This material is available free of charge via the Internet at http://pubs.acs.org.

## AUTHOR INFORMATION

### Corresponding Author

*Fax: +86-551-63601592. E-mail: hqyu@ustc.edu.cn.

### Notes

The authors declare no competing financial interest.

## ACKNOWLEDGMENTS

This work is supported by the National Basic Research Program of China (Grant 2011CB933700) and the Program for Changjiang Scholars and Innovative Research Team in University of the Ministry of Education of China.

## REFERENCES

(1) Novoselov, K. S.; Geim, A. K.; Morozov, S. V.; Jiang, D.; Zhang, Y.; Dubonos, S. V.; Grigorieva, I. V.; Firsov, A. A. Electric Field Effect in Atomically Thin Carbon Films. *Science* **2004**, *306*, 666–669.

(2) Chen, D.; Tang, L.; Li, J. Graphene-Based Materials in Electrochemistry. *Chem. Soc. Rev.* **2010**, *39*, 3157–3180.

(3) Huang, X.; Qi, X.; Boey, F.; Zhang, H. Graphene-Based Composites. *Chem. Soc. Rev.* **2012**, *41*, 666–686.

(4) Huang, Y.; Liang, J.; Chen, Y. An Overview of the Applications of Graphene-Based Materials in Supercapacitors. *Small* **2012**, *8*, 1805–1834.

(5) Stoller, M. D.; Park, S.; Zhu, Y.; An, J.; Ruoff, R. S. Graphene-Based Ultracapacitors. *Nano Lett.* **2008**, *8*, 3498–3502.

(6) Guo, S.; Dong, S.; Wang, E. Three-Dimensional Pt-on-Pd Bimetallic Nanodendrites Supported on Graphene Nanosheet: Facile Synthesis and Used as an Advanced Nanoelectrocatalyst for Methanol Oxidation. *ACS Nano* **2009**, *4*, 547–555.

(7) Huang, J.; Zhang, L.; Chen, B.; Ji, N.; Chen, F.; Zhang, Y.; Zhang, Z. Nanocomposites of Size-Controlled Gold Nanoparticles and Graphene Oxide: Formation and Applications in SERS and Catalysis. *Nanoscale* **2010**, *2*, 2733–2738.

(8) Lambert, T. N.; Chavez, C. A.; Hernandez-Sanchez, B.; Lu, P.; Bell, N. S.; Ambrosini, A.; Friedman, T.; Boyle, T. J.; Wheeler, D. R.; Huber, D. L. Synthesis and Characterization of Titania–Graphene Nanocomposites. *J. Phys. Chem. C* **2009**, *113*, 19812–19823.

(9) Li, Y.; Wang, H.; Xie, L.; Liang, Y.; Hong, G.; Dai, H. $MoS_2$ Nanoparticles Grown on Graphene: An Advanced Catalyst for the Hydrogen Evolution Reaction. *J. Am. Chem. Soc.* **2011**, *133*, 7296–7299.

(10) Liu, Z.; Liu, Q.; Huang, Y.; Ma, Y.; Yin, S.; Zhang, X.; Sun, W.; Chen, Y. Organic Photovoltaic Devices Based on a Novel Acceptor Material: Graphene. *Adv. Mater.* **2008**, *20*, 3924–3930.

(11) Seger, B.; Kamat, P. V. Electrocatalytically Active Graphene–Platinum Nanocomposites. Role of 2-D Carbon Support in PEM Fuel Cells. *J. Phys. Chem. C* **2009**, *113*, 7990–7995.

(12) Wang, H.; Casalongue, H. S.; Liang, Y.; Dai, H. $Ni(OH)_2$ Nanoplates Grown on Graphene as Advanced Electrochemical Pseudocapacitor Materials. *J. Am. Chem. Soc.* **2010**, *132*, 7472–7477.

(13) Guo, S.; Sun, S. FePt Nanoparticles Assembled on Graphene as Enhanced Catalyst for Oxygen Reduction Reaction. *J. Am. Chem. Soc.* **2012**, *134*, 2492–2495.

(14) Guo, S.; Zhang, S.; Wu, L.; Sun, S. Co/CoO Nanoparticles Assembled on Graphene for Electrochemical Reduction of Oxygen. *Angew. Chem., Int. Ed.* **2012**, *51*, 11770–11773.

(15) Li, F.; Yang, H.; Shan, C.; Zhang, Q.; Han, D.; Ivaska, A.; Niu, L. The Synthesis of Perylene-Coated Graphene Sheets Decorated with Au Nanoparticles and Its Electrocatalysis toward Oxygen Reduction. *J. Mater. Chem.* **2009**, *19*, 4022–4025.

(16) Liang, Y.; Li, Y.; Wang, H.; Zhou, J.; Wang, J.; Regier, T.; Dai, H. $Co_3O_4$ Nanocrystals on Graphene as a Synergistic Catalyst for Oxygen Reduction Reaction. *Nat. Mater.* **2011**, *10*, 780–786.

(17) Yoo, E.; Okata, T.; Akita, T.; Kohyama, M.; Nakamura, J.; Honma, I. Enhanced Electrocatalytic Activity of Pt Subnanoclusters on Graphene Nanosheet Surface. *Nano Lett.* **2009**, *9*, 2255–2259.

(18) Wang, Q. J.; Che, J. G. Origins of Distinctly Different Behaviors of Pd and Pt Contacts on Graphene. *Phys. Rev. Lett.* **2009**, *103*, 066802.
(19) Giovannetti, G.; Khomyakov, P.; Brocks, G.; Karpan, V.; van den Brink, J.; Kelly, P. Doping Graphene with Metal Contacts. *Phys. Rev. Lett.* **2008**, *101*, 026803.
(20) Cao, A.; Liu, Z.; Chu, S.; Wu, M.; Ye, Z.; Cai, Z.; Chang, Y.; Wang, S.; Gong, Q.; Liu, Y. A Facile One-Step Method to Produce Graphene−CdS Quantum Dot Nanocomposites as Promising Optoelectronic Materials. *Adv. Mater.* **2010**, *22*, 103−106.
(21) Chen, X.; Wu, G.; Chen, J.; Chen, X.; Xie, Z.; Wang, X. Synthesis of "Clean" and Well-Dispersive Pd Nanoparticles with Excellent Electrocatalytic Property on Graphene Oxide. *J. Am. Chem. Soc.* **2011**, *133*, 3693−3695.
(22) Gu, H.; Yang, Y.; Tian, J.; Shi, G. Photochemical Synthesis of Noble Metal (Ag, Pd, Au, Pt) on Graphene/ZnS Multihybrid Nanoarchitectures as Electrocatalysis for $H_2O_2$ Reduction. *ACS Appl. Mater. Interfaces* **2013**, *5*, 6762−6768.
(23) Huang, X.; Li, S.; Huang, Y.; Wu, S.; Zhou, X.; Li, S.; Gan, C. L.; Boey, F.; Mirkin, C. A.; Zhang, H. Synthesis of Hexagonal Close-Packed Gold Nanostructures. *Nat. Commun.* **2011**, *2*, 292−297.
(24) Kim, Y.-T.; Han, J. H.; Hong, B. H.; Kwon, Y.-U. Electrochemical Synthesis of CdSe Quantum-Dot Arrays on a Graphene Basal Plane Using Mesoporous Silica Thin-Film Templates. *Adv. Mater.* **2010**, *22*, 515−518.
(25) Moussa, S.; Abdelsayed, V.; Samy El-Shall, M. Laser Synthesis of Pt, Pd, CoO and Pd−CoO Nanoparticle Catalysts Supported on Graphene. *Chem. Phys. Lett.* **2011**, *510*, 179−184.
(26) Moussa, S.; Siamaki, A. R.; Gupton, B. F.; El-Shall, M. S. Pd-Partially Reduced Graphene Oxide Catalysts (Pd/PRGO): Laser Synthesis of Pd Nanoparticles Supported on PRGO Nanosheets for Carbon−Carbon Cross Coupling Reactions. *ACS Catal.* **2012**, *2*, 145−144.
(27) Ng, Y. H.; Iwase, A.; Kudo, A.; Amal, R. Reducing Graphene Oxide on a Visible-Light $BiVO_4$ Photocatalyst for an Enhanced Photoelectrochemical Water Splitting. *J. Phys. Chem. Lett.* **2010**, *1*, 2607−2612.
(28) Yang, J.; Tian, C.; Wang, L.; Fu, H. An Effective Strategy for Small-Sized and Highly-Dispersed Palladium Nanoparticles Supported on Graphene with Excellent Performance for Formic Acid Oxidation. *J. Mater. Chem.* **2011**, *21*, 3384−3390.
(29) Abdelsayed, V.; Moussa, S.; Hassan, H. M.; Aluri, H. S.; Collinson, M. M.; El-Shall, M. S. Photothermal Deoxygenation of Graphite Oxide with Laser Excitation in Solution and Graphene-Aided Increase in Water Temperature. *J. Phys. Chem. Lett.* **2010**, *1*, 2804−2809.
(30) Sokolov, D. A.; Shepperd, K. R.; Orlando, T. M. Formation of Graphene Features from Direct Laser-Induced Reduct Ion of Graphite Oxide. *J. Phys. Chem. Lett.* **2010**, *1*, 2633−2636.
(31) Yang, L.-C.; Lai, Y.-S.; Tsai, C.-M.; Kong, Y.-T.; Lee, C.-I.; Huang, C.-L. One-Pot Synthesis of Monodispersed Silver Nanodecahedra with Optimal SERS Activities Using Seedless Photo-Assisted Citrate Reduction Method. *J. Phys. Chem. C* **2012**, *116*, 24292−24300.
(32) Yao, K. X.; Liu, X.; Zhao, L.; Zeng, H. C.; Han, Y. Site-Specific Growth of Au Particles on ZnO Nanopyramids under Ultraviolet Illumination. *Nanoscale* **2011**, *3*, 4195−4200.
(33) Hummers, W. S.; Offeman, R. E. Preparation of Graphitic Oxide. *J. Am. Chem. Soc.* **1958**, *80*, 1339.
(34) Poh, H. L.; Sanek, F.; Ambrosi, A.; Zhao, G.; Sofer, Z.; Pumera, M. Graphenes Prepared by Staudenmaier, Hofmann and Hummers Methods with Consequent Thermal Exfoliation Exhibit Very Different Electrochemical Properties. *Nanoscale* **2012**, *4*, 3515−3522.
(35) Fang, L.-L.; Tao, Q.; Li, M.-F.; Liao, L.-W.; Chen, D.; Chen, Y.-X. Determination of the Real Surface Area of Palladium Electrode. *Chin. J. Chem. Phys.* **2010**, *23*, 543−548.
(36) Stankovich, S.; Piner, R. D.; Chen, X.; Wu, N.; Nguyen, S. T.; Ruoff, R. S. Stable Aqueous Dispersions of Graphitic Nanoplatelets Via the Reduction of Exfoliated Graphite Oxide in the Presence of Poly(Sodium 4-Styrenesulfonate). *J. Mater. Chem.* **2006**, *16*, 155.
(37) Stankovich, S.; Dikin, D. A.; Piner, R. D.; Kohlhaas, K. A.; Kleinhammes, A.; Jia, Y.; Wu, Y.; Nguyen, S. T.; Ruoff, R. S. Synthesis of Graphene-Based Nanosheets Via Chemical Reduction of Exfoliated Graphite Oxide. *Carbon* **2007**, *45*, 1558−1565.
(38) Su, S. C.; Carstens, J. N.; Bell, A. T. A Study of the Dynamics of Pd Oxidation and PdO Reduction by $H_2$ and $CH_4$. *J. Catal.* **1998**, *176*, 125−135.
(39) Baylet, A.; Marecot, P.; Duprez, D.; Castellazzi, P.; Groppi, G.; Forzatti, P. In situ Raman and in situ XRD Analysis of PdO Reduction and Pd Degrees Oxidation Supported on Gamma-$Al_2O_3$ Catalyst under Different Atmospheres. *Phys. Chem. Chem. Phys.* **2011**, *13*, 4607−4613.
(40) Stankovich, S.; Piner, R. D.; Nguyen, S. T.; Ruoff, R. S. Synthesis and Exfoliation of Isocyanate-Treated Graphene Oxide Nanoplatelets. *Carbon* **2006**, *44*, 3342−3347.
(41) Lim, B.; Xiong, Y.; Xia, Y. A Water-Based Synthesis of Octahedral, Decahedral, and Icosahedral Pd Nanocrystals. *Angew. Chem.* **2007**, *119*, 9439−9442.
(42) Liu, X.; Li, L.; Meng, C.; Han, Y. Palladium Nanoparticles/Defective Graphene Composites as Oxygen Reduction Electrocatalysts: A First-Principles Study. *J. Phys. Chem. C* **2012**, *116*, 2710−2719.
(43) Yin, H.; Tang, H.; Wang, D.; Gao, Y.; Tang, Z. Facile Synthesis of Surfactant-Free Au Cluster/Graphene Hybrids for High-Performance Oxygen Reduction Reaction. *ACS Nano* **2012**, *6*, 8288−8297.
(44) Jin, T.; Guo, S.; Zuo, J. L.; Sun, S. Synthesis and Assembly of Pd Nanoparticles on Graphene for Enhanced Electrooxidation of Formic Acid. *Nanoscale* **2013**, *5*, 160−163.
(45) Santasalo-Aarnio, A.; Kwon, Y.; Ahlberg, E.; Kontturi, K.; Kallio, T.; Koper, M. T. M. Comparison of Methanol, Ethanol and Iso-Propanol Oxidation on Pt and Pd Electrodes in Alkaline Media Studied by HPLC. *Electrochem. Commun.* **2011**, *13*, 466−469.
(46) Liu, X.; Meng, C.; Han, Y. Defective Graphene Supported $MPd_{12}$ (M = Fe, Co, Ni, Cu, Zn, Pd) Nanoparticles as Potential Oxygen Reduction Electrocatalysts: A First-Principles Study. *J. Phys. Chem. C* **2013**, *117*, 1350−1357.
(47) Liu, M.; Zhang, R.; Chen, W. Graphene-Supported Nanoelectrocatalysts for Fuel Cells: Synthesis, Properties, and Applications. *Chem. Rev.* **2014**, *114*, 5117−5160.